Formation of Gapless Fermi Arcs and Fingerprints of Order in the Pseudogap State of Cuprate Superconductors

Takeshi Kondo,[1,*] Ari D. Palczewski,[1] Yoichiro Hamaya,[2] Tsunehiro Takeuchi,[2,3] J. S. Wen,[4] Z. J. Xu,[4] Genda Gu,[4] and Adam Kaminski[1]

[1]*Ames Laboratory and Department of Physics and Astronomy, Iowa State University, Ames, Iowa 50011, USA*
[2]*Department of Crystalline Materials Science, Nagoya University, Nagoya 464-8603, Japan*
[3]*EcoTopia Science Institute, Nagoya University, Nagoya 464-8603, Japan*
[4]*Condensed Matter Physics and Materials Science Department, Brookhaven National Laboratory, Upton, New York 11973, USA*

(Received 25 March 2013; published 8 October 2013)

We use angle-resolved photoemission spectroscopy and a new quantitative approach based on the partial density of states to study properties of seemingly disconnected portions of the Fermi surface (FS) that are present in the pseudogap state of cuprates called Fermi arcs. We find that the normal state FS collapses very abruptly into Fermi arcs at the pseudogap temperature (T^*). Surprisingly, the length of the Fermi arcs remains constant over an extended temperature range between T^* and T_{pair}, consistent with the presence of an ordered state below T^*. These arcs collapse again at the temperature below which pair formation occurs (T_{pair}) either to a point or a very short arc, whose length is limited by our experimental resolution. The tips of the arcs span between points defining a set of wave vectors in momentum space, which are the fingerprints of the ordered state that causes the pseudogap.

DOI: 10.1103/PhysRevLett.111.157003 PACS numbers: 74.70.Dd, 71.18.+y, 71.20.−b, 71.27.+a

The Fermi surface in the pseudogap [1–15] state of the cuprates is highly unusual because it appears to consist of disconnected segments called Fermi arcs [16]. Their very existence challenges the traditional concept of a Fermi surface as closed contours of gapless excitations in momentum space. A linear increase of arc length with temperature [14,17] was interpreted as an interplay of a d-wave pairing gap [18] and strong scattering [19]. In such a case, the Fermi arcs [16] are not real, gapless portions of a normal state Fermi surface [20]. This picture was recently confirmed by spectroscopic evidence that a d-wave gap [20] and pairing [21] are present above T_c up to 150 K. It is not clear whether the Fermi arcs remain gapless above this temperature. Traditional methods for determining the presence of an energy gap in angle-resolved photoemission spectroscopy (ARPES) spectra [5,6,16,17] rely on a line shape analysis such as a shift in the leading edge or a dip in symmetrized spectra [16]. In the cuprates, however, these features are poorly defined (especially above T_c) because the spectral peaks are very broad in optimally and underdoped samples. More importantly, this approach is strongly affected by the lifetime effects, which likely explain linear variation of such determined arcs with temperature [17,19]. This makes the detection of very small energy gaps and partial gaps (such as the pseudogap, which affects only part of the spectral weight) difficult or impossible to do. An energy gap is most precisely defined as a decrease of the density of states [DOS(E_F)] at the Fermi energy. Such a quantity provides also one of the most sensitive ways to detect of the opening of an energy gap. In a gapless state, this quantity is independent of temperature because unlike the spectral function, it does not depend on the electron lifetime. The opening of an energy gap at the Fermi energy leads to a decrease of DOS(E_F). Studying this quantity as a function of temperature therefore provides a very sensitive method to detect an opening of the energy gap, which is objective and independent of the scattering effects. To obtain momentum dependent information, one can use the area of the momentum distribution curve (MDC) at the Fermi energy [$A_{\text{MDC}}(E_F)$] along a cut in momentum space, which represents a contribution to the DOS(E_F) from a small slice of the Brillouin zone. One can make an even more rigorous argument, since the MDCs in cuprates, in the absence of an energy gap, are well described by a Lorentzian line shape [22–24], and their area is independent of scattering and temperature. The opening of an energy gap lowers the spectral intensity at E_F and therefore decreases the $A_{\text{MDC}}(E_F)$ (see a simple simulation in Fig. S6 in the Supplemental Material [25]).

In this Letter, we use this novel approach, based on the temperature dependence of the density of states, to detect the opening of an energy gap in cuprates. This requires very high quality data and temperature stability, but at the same time, it allows us to obtain momentum-resolved information about the opening of an energy gap with significantly higher accuracy than previously possible. We demonstrate that real, gapless Fermi arcs exist above 150 K ($>T_c$) and their length remains surprisingly constant up to the pseudogap temperature T^*, where a closed contour, normal state Fermi surface is recovered. This finding resolves the controversy about the nature of arcs and presents a consistent picture of fermiology in the pseudogap state of cuprates. The tips of the arcs connect

fixed points in momentum space and define a set of wave vectors, which are the fingerprints of the ordered state that causes the pseudogap.

Optimally doped $Bi_2Sr_2CaCu_2O_{8+\delta}$ (Bi2212) single crystals with $T_c = 93$ K (OP93K) and $(Bi, Pb)_2 \times (Sr, La)_2CuO_{6+\delta}$ (Bi2201) single crystals with $T_c = 32$ K (OP32K) were grown by the conventional floating-zone technique [26]. The samples were cleaved *in situ* at base pressure lower than 3×10^{-11} Tr, yielding shiny, flat, mirrorlike surfaces. ARPES data were acquired using a laboratory-based system consisting of a Scienta SES2002 electron analyzer and a Gammadata helium UV lamp. All data were acquired using the HeI line with a photon energy of 21.2 eV. The angular resolution was 0.13° (~ 0.005 Å^{-1}) and ~0.5° (0.019 Å^{-1}) along and perpendicular to the direction of the analyzer slits, respectively, and it was independent of the temperature in our experimental setup. The energy corresponding to the chemical potential was determined from the Fermi edge of a polycrystalline Au reference in electrical contact with the sample. The energy resolution was set at ~10 meV. Custom designed refocusing optics enabled us to accumulate high statistics spectra in a short period of time with no sample surface aging from the absorption or loss of oxygen. Measurements were performed on several samples, and we confirmed that all yielded consistent results. Additional details are presented in the Supplemental Material [25].

In Fig. 1, we demonstrate the above procedure using data at the node (gapless) and away from the node (gapped) from a Bi2201 sample and compare it to the traditional method of symmetrization. Figure 1(a) shows the MDCs along the nodal cut [see the inset of Fig. 1(b)] measured at various temperatures from below the superconducting transition temperature (T_c) to above the T^*. The MDC peak, which is observed at k_F, broadens with increased temperature, and peak intensity decreases, as the electron lifetime shortens due to scattering. To make a better comparison of data at various momentum points, we express the area of the MDCs $A_{\mathrm{MDC}}(E_F)$ as a percentage of the normal state area. In the case of a nodal cut, this quantity remains constant at ~100% for all temperatures, as expected for a partial contribution to the DOS in the absence of an energy gap [Fig. 1(b)]. This behavior changes dramatically away from the node, where an energy gap opens. Figure 1(c) shows the MDCs along a momentum cut close to the antinode [see the inset of Fig. 1(d)]. At high temperatures above T^*, the peak width increases, peak intensity decreases, and the MDC area remains constant, as expected. Below T^*, the peak intensity and area begin to decrease with decreasing temperature, indicating the opening of an energy gap. This is even more evident in Fig. 1(d), which shows the $A_{\mathrm{MDC}}(E_F)$ as a function of temperature. This quantity is constant at high temperatures and decreases below T^*. The reduction of $A_{\mathrm{MDC}}(E_F)$ below T^* signifies the opening of an energy gap—in this case, the pseudogap (arrow). The extraordinary sensitivity of this DOS-based method allows us to detect smaller gaps at higher temperatures. This results in a more accurate determination of T^* that is 30–40 K higher for the same batch of

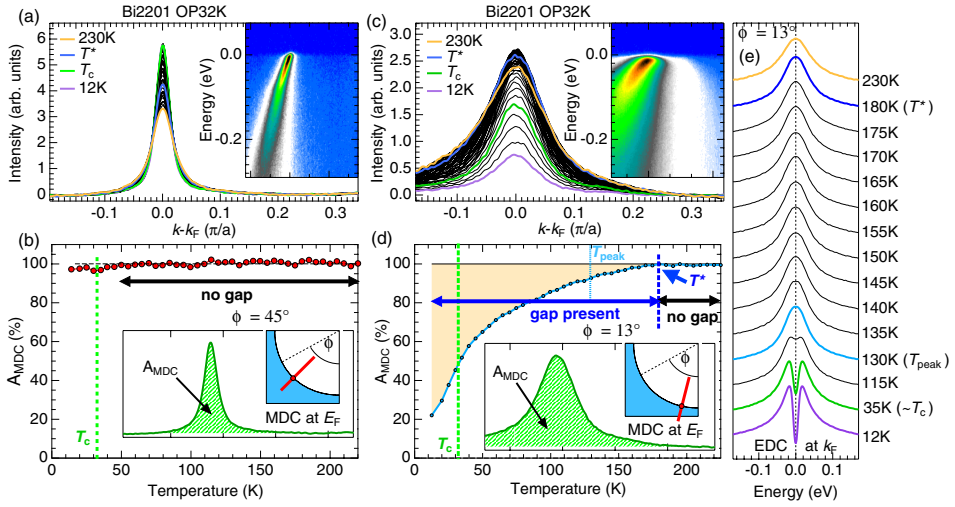

FIG. 1 (color online). Determination of the partial density of states at E_F, $A_{\mathrm{MDC}}(E_F)$, from the ARPES data of optimally doped Bi2201 ($T_c = 32$ K). (a) MDCs measured along the nodal direction. The inset shows a dispersion image at the lowest temperature (12 K). (b) The temperature dependence of $A_{\mathrm{MDC}}(E_F)$ estimated from the area of MDCs in (a). The momentum cut and estimated area of MDC are shown in the inset. Statistical error bars are smaller than the size of the symbols, and the main source of noise in the data is stability of the ARPES spectrometer, which can be evaluated by the small scatter of the data points. (c) Same data as in (a), but measured along a momentum cut slightly off the antinode. (d) The temperature dependence of $A_{\mathrm{MDC}}(E_F)$ estimated from the area of MDCs in (c). (e) Symmetrized EDCs at k_F for several temperatures, obtained from the data of (c). The T_{peak} is defined as the temperature where two peaks in the spectrum merge to one peak at elevated temperatures.

samples than in our previous work [21] based on the line shape criterion.

For a comparison, we plot the symmetrized energy distribution curves (EDCs) at k_F for several temperatures in Fig. 1(e). This is the traditional way to detect the energy gap [16,17]. The single peak present at high temperatures develops a dip on cooling (below the temperature marked as $T_{\rm peak}$), which was previously interpreted as a signature of a gap opening. It is clear that the $T_{\rm peak}$ is considerably lower than the T^* because smaller gaps, even if present, do not always produce a dip in the symmetrized spectra. Careful investigation of $A_{\rm MDC}(E_F, T)$ is essential to detect the temperature at which energy gap(s) open. We also note that in the scanning tunneling spectroscopy data, the dip at E_F exists above $T_{\rm peak}$ (previously considered to be the pseudogap opening temperature) [27,28].

In order to study the temperature evolution of the Fermi arc, we carefully measured $A_{\rm MDC}(E_F, T)$ for a number of Fermi momentum points. In Fig. 2, we show the data obtained from optimally doped Bi2201 ($T_c = 32$ K; raw MDC data are included in the Supplemental Material [25]). The $A_{\rm MDC}(E_F, T)$ starts to decrease upon cooling at T^* in the top four panels for $0° \le \phi \le 17°$, indicated by arrows. This signifies the simultaneous opening of the pseudogap for a range of Fermi momentum points up to $\phi \le 19°$ at T^*. The Fermi surface therefore collapses very abruptly at T^*. For the Fermi momentum points closer to the node (bottom four panels), the $A_{\rm MDC}(E_F, T)$ remains constant down to a much lower temperature, the value of which is the same as the onset of pairing [21]—$T_{\rm pair}$. The lack of variation in $A_{\rm MDC}(E_F, T)$ for $\phi > 19°$ down to $T_{\rm pair}$ demonstrates the absence of a gap and indicates that the length of the arcs is constant in this temperature range. On further cooling, at $T_{\rm pair}$, $A_{\rm MDC}(E_F, T)$ starts to simultaneously decrease at four measured points on the arc [marked by arrows in Figs. 2(e)–2(h)]. This signifies the collapse of the arcs below $T_{\rm pair}$ into the point node of a d-wave paired state. The same behavior, albeit with slightly different values of $T_{\rm pair}$ and momenta, is observed in optimally doped Bi2212 samples ($T_c = 93$ K), as shown in Fig. 3.

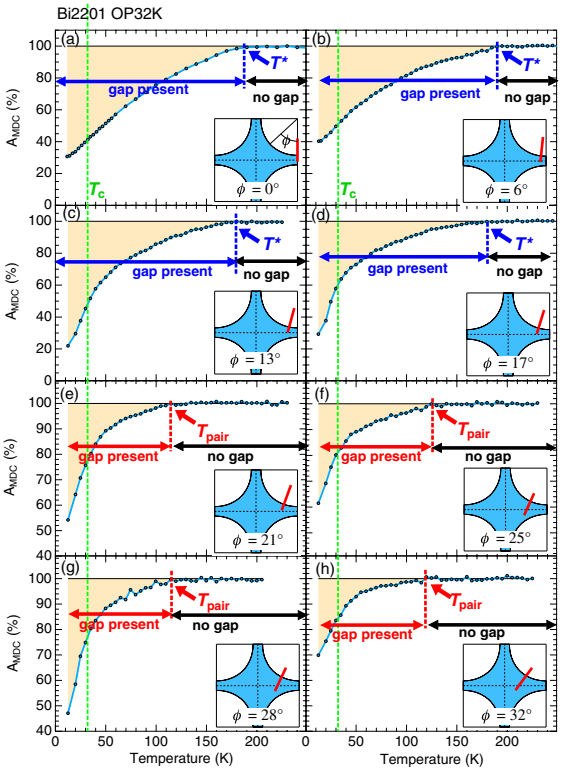

FIG. 2 (color online). Temperature dependence of the MDC area along the Fermi surface $A_{\rm MDC}(E_F)$ for optimally doped Bi2201 ($T_c = 32$ K) measured at several points on the Fermi surface. $A_{\rm MDC}(E_F)$ is expressed as a percentage of the MDC area above T^*. The top left panel corresponds to the antinodal direction. The inset of each panel shows the FS and the location of the cut, normal to the FS. The pseudogap temperature (T^*) and the temperature above which the arc exists ($T_{\rm pair}$) are indicated by arrows. T_c is indicated by a dotted green line. $A_{\rm MDC}(E_F)$ at the nodal point is constant down to lowest temperature and already shown in Fig. 1(b).

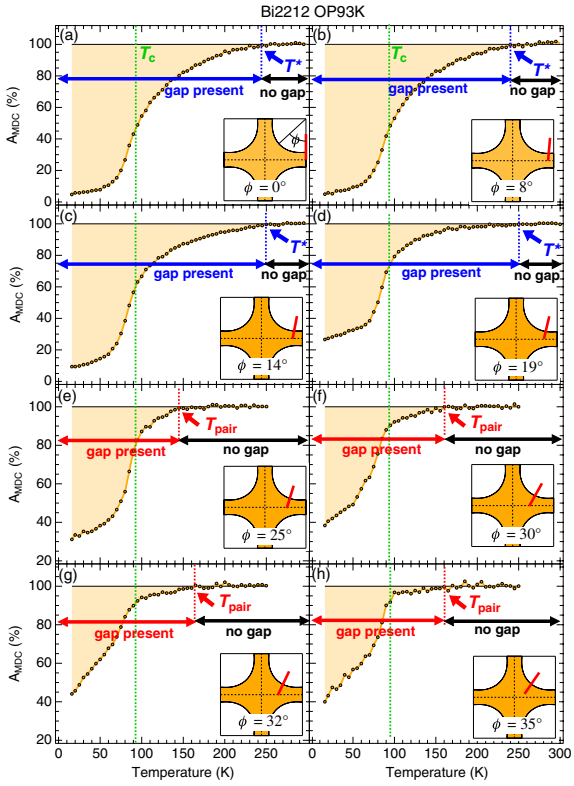

FIG. 3 (color online). Temperature dependence of the MDC area along the Fermi surface $A_{\rm MDC}(E_F)$ for optimally doped Bi2212 with $T_c = 93$ K measured at several points on the Fermi surface similarly to Fig. 2. The pseudogap temperature (T^*) and the temperature above which the arc exists ($T_{\rm pair}$) are indicated by arrows. T_c is indicated by a dotted green line. $A_{\rm MDC}(E_F)$ at the nodal point is constant down to the lowest temperature and shown in Fig. S5 of the Supplemental Material [25].

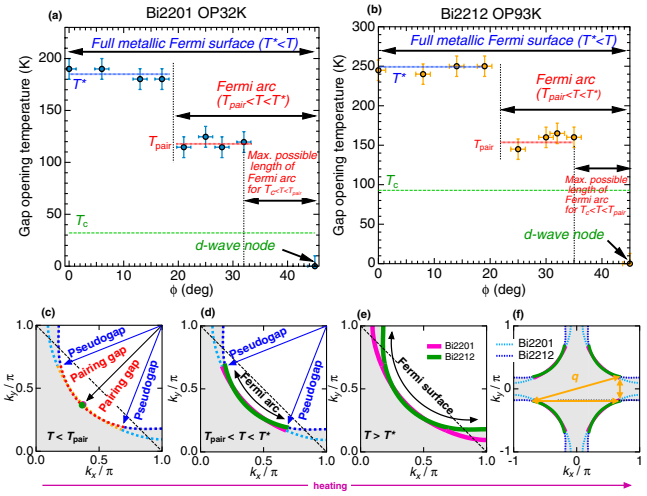

FIG. 4 (color online). Momentum dependence of the temperatures at which the gap opens and the length of the Fermi arc is determined from ARPES data and marked by red and blue arrows in Figs. 2 and 3 (a) for optimally doped Bi2201 and (b) for optimally doped Bi2212. The length of the arcs remains constant for $T_{\rm pair} < T < T^*$. Below $T_{\rm pair}$, we can only impose an upper limit on the length of the remaining arc indicated by black arrows. (c)–(e) The Fermi surface for three key temperature ranges. The antiferromagnetic zone boundary is marked with a dashed black line. (f) The Fermi arcs of the Bi2212 and Bi2201 samples for $T_{\rm pair} < T < T^*$ determined from our ARPES data. The key q vectors connecting the tips of the Fermi arcs are indicated with arrows.

We note that there several features present in $A_{\rm MDC}$ data below the temperature at which the gap opens. Most notably, there is an accelerated decrease of the $A_{\rm MDC}(E_F)$ in already gapped parts of the Fermi surface (FS) (ϕ values of 6° or 13° for Bi2201 or 8°, 14°, and 19° for Bi2212) below a temperature that coincides with $T_{\rm pair}$. Naturally, the formation of a d-wave pairing gap [20,21] below that temperature would cause a faster decrease of the density of states at E_F. A number of other features seen in the data can be attributed to changes of the electron scattering rate. The area of MDC is not affected by the scattering only in the absence of an energy gap and therefore can be used to detect such an event. Once an energy gap is present, this is no longer true, and changes in the scattering rate will affect the $A_{\rm MDC}(E_F)$. This likely contains a lot of important information about pairing, but its understanding would need significant theoretical consideration, which is beyond the scope of the present work and will be studied carefully in the future.

We summarize key results in Fig. 4. In Figs. 4(a) and 4(b), we plot the gap opening temperatures for Bi2201 and Bi2212, respectively. These are the temperatures indicated by arrows in Figs. 2 and 3, which mark the onset of a decrease in $A_{\rm MDC}(E_F, T)$ and therefore the opening of an energy gap. In the antinodal region, for $\phi \lesssim 20°$, this occurs at T^*, below which a gapless arc is present. The four momentum points on the arc remain gapless down to $T_{\rm pair}$, which means that the length of the arc is roughly constant and equal to ~60% of the normal state FS between T^* and $T_{\rm pair}$. Below $T_{\rm pair}$ [indicated by the arrows in Figs. 2(e)–2(h) and 3(e)–3(h)], the gap opens simultaneously for all four momentum points on the arc we measured. Therefore, that portion of the arc collapses below this temperature. Using our method close to the node (i.e., $\phi \gtrsim 35°$) is difficult because the gap magnitude is very small and its effects on the DOS are below current sensitivity. Therefore, we can only impose an upper limit on the length of the remaining arc for $T < T_{\rm pair}$ of 20%–30%, as indicated in each panel of Fig. 4; however, a separate set of experiments [20,21] strongly suggests that the d-wave pairing gap is present below 150 K (Bi2212), and therefore real arcs are collapsed to a node. In Figs. 4(c)–4(e), we present a schematic diagram demonstrating the process of forming the arcs and their subsequent collapse. Our most important finding is the collapse of the Fermi surface into arcs on cooling at T^* and the constant length of these arcs down to $T_{\rm pair}$. We emphasize that the traditional line shape analysis underestimates the temperature at which an energy gap opens due to scattering effects. To confirm this, we repeated a traditional symmetrization analysis for our data from Figs. 2 and 3 and demonstrated an apparent linear expansion of the arcs with temperature (see the Supplemental Material [25]).

We note that the Fermi momentum points at the tips of the arcs do not coincide with the antiferromagnetic zone boundary. The vectors connecting these points such as (0, 0.4), (1.4, 0), and (1.4, 0.4) are likely the key to determining the nature of the ordered state underlying the pseudogap phenomenon in the cuprates. This finding is consistent with the presence of an ordered state below T^* and/or elusive Fermi pockets [29,30]. Earlier STM studies [31,32] proposed a scenario for the pseudogap based on a charge density wave with a (0, 0.4) ordering vector. We note that in the case of Bi2201, the FS segments close to the antinode are not parallel and are not significantly nested [33]. The strong energy dependence of the checkerboard pattern [34] in STM is also inconsistent with the signatures of a classical charge density wave. The other two vectors, however, may be related to a nematic state reported by a separate STM study [35]. So far, we have not been able to identify a theory consistent with the above set of vectors; however, we hope that this information will lead to the development of a correct theory of the pseudogap state.

We thank Mike Norman, Jörg Schmalian, and Andrey V. Chubukov for useful discussions. This work was supported by Basic Energy Sciences, U.S. DOE. T. K. is supported by JSPS (KAKENHI Contract No. 24740218). The Ames Laboratory is operated for the U.S. DOE by Iowa State University under Contract No. DE-AC02-07CH11358.

Work at Brookhaven is supported by the U.S. DOE under Contract No. DE-AC02-98CH10886. J. S. W. and Z. J. X. are supported by the Center for Emergent Superconductivity, an Energy Frontier Research Center funded by the U.S. DOE, Office of Science.

*Current address: Institute for Solid State Physics, University of Tokyo, Kashiwa, Chiba 277-8581, Japan.

[1] W. W. Warren, Jr., R. E. Walstedt, G. F. Brennert, R. J. Cava, R. Tycko, R. F. Bell, and G. Dabbagh, Phys. Rev. Lett. **62**, 1193 (1989).
[2] M. Takigawa, A. P. Reyes, P. C. Hammel, J. D. Thompson, R. H. Heffner, Z. Fisk, and K. C. Ott, Phys. Rev. B **43**, 247 (1991).
[3] C. C. Homes, T. Timusk, R. Liang, D. A. Bonn, and W. N. Hardy, Phys. Rev. Lett. **71**, 1645 (1993).
[4] D. N. Basov, H. A. Mook, B. Dabrowski, and T. Timusk, Phys. Rev. B **52**, R13141 (1995).
[5] H. Ding, T. Yokoya, J. C. Campuzano, T. Takahashi, M. Randeria, M. R. Norman, T. Mochiku, K. Kadowaki, and J. Giapintzakis, Nature (London) **382**, 51 (1996).
[6] A. G. Loeser, Z.-X. Shen, D. S. Dessau, D. S. Marshall, C. H. Park, P. Fournier, and A. Kapitulnik, Science **273**, 325 (1996).
[7] M. R. Norman, D. Pines, and C. Kallin, Adv. Phys. **54**, 715 (2005).
[8] V. J. Emery and S. A. Kivelson, Nature (London) **374**, 434 (1995).
[9] J. Lee, K. Fujita, A. R. Schmidt, C. K. Kim, H. Eisaki, S. Uchida, and J. C. Davis, Science **325**, 1099 (2009).
[10] K. Tanaka *et al.*, Science **314**, 1910 (2006).
[11] M. Le Tacon, A. Sacuto, A. Georges, G. Kotliar, Y. Gallais, D. Colson, and A. Forget, Nat. Phys. **2**, 537 (2006).
[12] T. Kondo, T. Takeuchi, A. Kaminski, S. Tsuda, and S. Shin, Phys. Rev. Lett. **98**, 267004 (2007).
[13] T. Kondo, R. Khasanov, T. Takeuchi, J. Schmalian, and A. Kaminski, Nature (London) **457**, 296 (2009).
[14] U. Chatterjee *et al.*, Nat. Phys. **6**, 99 (2009).
[15] H.-B. Yang, J. D. Rameau, P. D. Johnson, T. Valla, A. Tsvelik, and G. D. Gu, Nature (London) **456**, 77 (2008).
[16] M. R. Norman *et al.*, Nature (London) **392**, 157 (1998).
[17] A. Kanigel *et al.*, Nat. Phys. **2**, 447 (2006).
[18] T. Valla, A. V. Fedorov, J. Lee, J. C. Davis, and G. D. Gu, Science **314**, 1914 (2006).
[19] A. V. Chubukov, M. R. Norman, A. J. Millis, and E. Abrahams, Phys. Rev. B **76**, 180501 (2007).
[20] T. J. Reber *et al.*, Nat. Phys. **8**, 606 (2012).
[21] T. Kondo, Y. Hamaya, A. D. Palczewski, T. Takeuchi, J. S. Wen, Z. J. Xu, G. Gu, J. Schmalian, and A. Kaminski, Nat. Phys. **7**, 21 (2010).
[22] T. Valla, A. V. Fedorov, P. D. Johnson, B. O. Wells, S. L. Hulbert, Q. Li, G. D. Gu, and N. Koshizuka, Science **285**, 2110 (1999).
[23] A. Kaminski, M. Randeria, J. C. Campuzano, M. R. Norman, H. Fretwell, J. Mesot, T. Sato, T. Takahashi, and K. Kadowaki, Phys. Rev. Lett. **86**, 1070 (2001).
[24] A. Kaminski *et al.*, Phys. Rev. B **71**, 014517 (2005).
[25] See Supplemental Material at http://link.aps.org/supplemental/10.1103/PhysRevLett.111.157003 for more details about sample preparation, experimental technique, verification of the normalization procedure, and a more extensive set of raw data.
[26] T. Kondo, T. Takeuchi, U. Mizutani, T. Yokoya, S. Tsuda, and S. Shin, Phys. Rev. B **72**, 024533 (2005).
[27] K. K. Gomes, A. N. Pasupathy, A. Pushp, S. Ono, Y. Ando, and A. Yazdani, Nature (London) **447**, 569 (2007).
[28] C. V. Parker, P. Aynajian, E. H. da Silva Neto, A. Pushp, S. Ono, J. Wen, Z. Xu, G. Gu, and A. Yazdani, Nature (London) **468**, 677 (2010).
[29] J. Meng *et al.*, Nature (London) **462**, 335 (2009).
[30] H.-B. Yang, J. D. Rameau, Z.-H. Pan, G. D. Gu, P. D. Johnson, H. Claus, D. G. Hinks, and T. E. Kidd, Phys. Rev. Lett. **107**, 047003 (2011).
[31] W. D. Wise, M. C. Boyer, K. Chatterjee, T. Kondo, T. Takeuchi, H. Ikuta, Y. Wang, and E. W. Hudson, Nat. Phys. **4**, 696 (2008).
[32] W. D. Wise *et al.*, Nat. Phys. **5**, 213 (2009).
[33] A. D. Palczewski *et al.*, Phys. Rev. B **78**, 054523 (2008).
[34] T. Hanaguri, C. Lupien, Y. Kohsaka, D.-H. Lee, M. Azuma, M. Takano, H. Takagi, and J. C. Davis, Nature (London) **430**, 1001 (2004).
[35] A. Mesaros, K. Fujita, H. Eisaki, S. Uchida, J. C. Davis, S. Sachdev, J. Zaanen, M. J. Lawler, and E.-A. Kim, Science **333**, 426 (2011).